

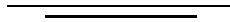
## LECTURE 1

## Coalescence of Binary Neutron Stars

K. Oohara<sup>(1)</sup> and T. Nakamura<sup>(2)</sup>

<sup>(1)</sup> *Department of Physics,  
Niigata University,  
Ikarashi, Niigata, 950-21,  
Japan*

<sup>(2)</sup> *Yukawa Institute for Theoretical Physics,  
Kyoto University,  
Kyoto, 606-01,  
Japan*



## 1. INTRODUCTION

The most important sources for laser-interferometric gravitational-wave detectors like LIGO or VIRGO are catastrophic events such as coalescence of a neutron-star binary. A binary system evolves quasi-stationarily and the wave pattern is regular up to the onset of coalescence. In *the last three minutes* of coalescing binaries, comparison of observed wave patterns with theoretical templates will hence make it possible to determine mass and spin of stars. In this phase, the post-Newtonian expansion will give good templates since  $v_{\text{rot}}/c$  is as small as 0.1. In the final phase of the coalescence, however, there is no such small parameters. Numerical relativity is one of methods for studying such nonlinear phase of coalescing binary neutron stars; we call it *the last three milliseconds*. In order to know the characteristics of the waves in the last three milliseconds, general relativistic (GR) calculations are required. However, coalescence of binary stars is a completely non-axisymmetric, 3 dimensional (in space) event and 3D GR calculation requires great powers of computers. We should hence make progress step by step. First of all, we used a Newtonian hydrodynamics code including radiation reaction of gravitational waves and

then we considered post-Newtonian correction, which is called (1+2.5) post-Newtonian calculation, since a radiation reaction potential is expressed as 2.5 post-Newtonian terms. These calculations give a lot of perspectives on gravitational wave patterns and dynamics of coalescing events. Finally we began to attack a 3D GR code for the final phase of coalescing binary neutron stars.

In this lecture, we describe results of numerical simulations of coalescing binary neutron stars using Newtonian and post-Newtonian hydrodynamics code and then discuss recent development of our 3D GR code for the last three milliseconds.

## 2. POST-NEWTONIAN SIMULATIONS

### 2.1. (1+2.5) Post-Newtonian Hydrodynamics Equations

The equations of motion including general relativistic effects up to order  $(v/c)^2$  is called the first post-Newtonian (1PN) approximation. However, gravitational damping effects start at order  $(v/c)^5$ , second-and-a-half post-Newtonian (2.5PN) terms, and the formulation for adding the effects to the equation of motion depends on the gauge condition. For example, the radiation reaction is represented by adding to the standard Newtonian potential a “radiation-reaction” potential proportional to the fifth time derivatives of the quadrupole moments [1].

In numerical calculations, however, it is hard to calculate the fifth time derivatives with satisfactory accuracy. Blanchet, Damour & Schäfer [2] presented (1+2.5)PN hydrodynamics equations including radiation damping effects, where we need up to the third time derivatives of the quadrupole moments. Following them, we use the evolution equations given by

$$\partial_t \rho + \partial_j (\rho v^j) = 0, \quad (1)$$

$$\partial_t (\rho w_i) + \partial_j (\rho w_i v^j) = F_i^{\text{press}} + F_i^{1\text{PN}} + F_i^{\text{reac}}, \quad (2)$$

$$\partial_t (\rho \varepsilon) + \partial_j (\rho \varepsilon v^j) = -p \partial_j v^j, \quad (3)$$

where  $\rho$ ,  $\varepsilon$  and  $p$  are the coordinate rest-mass density, the internal energy density and the pressure, respectively. In order to express a hard equation of state for a neutron star, we use a polytropic equation of motion

$$p = (\gamma - 1)\rho\varepsilon \quad (4)$$

with  $\gamma = 2$ . The quantity  $v^i$  denotes the 3-velocity and  $w_i$  is the “momentum per unit rest-mass.” In terms of  $w_i$ , the 3-velocity  $v^i$  is given by

$$v^i = \left(1 - \frac{\beta}{c^2}\right) w_i + \frac{1}{c^2} A_i + \frac{4G}{5c^5} w_j Q_{ij}^{[3]}, \quad (5)$$

where

$$Q_{ij}^{[3]} = \text{STF} \left\{ 2 \int [p \partial_i w_j - 2\rho w^i \partial_j \psi + x^i \partial_j \psi \partial_k (\rho w^k) - \rho x^i \partial_j \psi_t] dV \right\}, \quad (6)$$

which is the third time derivative of the reduced quadrupole moment of the system with the addition of corrections of order  $O(c^{-2})$  [3]. Here STF is the operator which takes the symmetric, trace-free part of any two-index object  $A^{ij}$ :

$$\text{STF} \{A^{ij}\} = \frac{1}{2}A^{ij} + \frac{1}{2}A^{ji} - \frac{1}{3}\delta^{ij}A^{kk}. \quad (7)$$

The forces are given by

$$\begin{aligned} F_i^{\text{press}} &= -\partial_i \left[ \left(1 + \frac{\alpha}{c^2}\right) p \right], \\ F_i^{1\text{PN}} &= -\rho \left[ \left(1 + \frac{\delta}{c^2}\right) \partial_i \psi + \frac{1}{c^2} \partial_i \psi_2 + \frac{1}{c^2} w_j \partial_i A_j \right], \\ F_i^{\text{reac}} &= -\frac{1}{c^5} \rho \partial_i \psi_r. \end{aligned} \quad (8)$$

Here  $\psi$  is the Newtonian potential,  $\alpha$ ,  $\beta$ ,  $\delta$ ,  $\psi_2$  and  $A_i$  are 1PN quantities and  $\psi_r$  is the radiation-reaction potential (a 2.5PN quantity):

$$\begin{aligned} \alpha &= (3\gamma - 2)\psi - \frac{1}{2}\gamma w^2, \\ \beta &= \frac{1}{2}w^2 + \gamma\varepsilon - 3\psi, \\ \delta &= \frac{3}{2}w^2 + (3\gamma - 2)\varepsilon + \psi, \\ A_i &= U_i - \frac{1}{2}x^i \psi_t, \\ \psi_r &= \frac{2}{5}G \left[ R - Q_{ij}^{[3]} x^i \partial_j \psi \right], \end{aligned} \quad (9)$$

where  $w^2 = \delta^{ij} w_i w_j$  and  $\psi_t$  is the time derivative of  $\psi$  with the addition of corrections of order  $O(c^{-2})$ . To compute  $\psi$ ,  $\psi_t$ ,  $\psi_2$ ,  $R$  and  $U_i$ , we must solve seven Poisson equations at each time step:

$$\Delta \psi = 4\pi G \rho, \quad (10)$$

$$\Delta \psi_t = -4\pi G \partial_j (\rho w_j), \quad (11)$$

$$\Delta \psi_2 = 4\pi G \rho \delta, \quad (12)$$

$$\Delta R = 4\pi G Q_{ij}^{[3]} x^i \partial_j \rho, \quad (13)$$

$$\Delta U_i = -4\pi G \left( 4\rho w_i + \frac{1}{2} x^i \partial_j (\rho w_j) \right). \quad (14)$$

The energy flux of the gravitational waves is given by

$$\frac{dE}{dt} = -\frac{G}{5c^5} Q_{ij}^{[3]} \frac{d}{dt} I_{ij}, \quad (15)$$

where

$$I_{ij} = \text{STF} \left\{ 2 \int \rho [w_i w_j - x^i \partial_j \psi] dV \right\}, \quad (16)$$

which is the second time derivative of the reduced quadrupole moment with the addition of corrections of order  $O(c^{-2})$ . The standard quadrupole formula gives the amplitude  $h_{ij}^{\text{TT}}$  of the gravitational waves in the transverse-traceless gauge [1]

$$h_{ij}^{\text{TT}} = \frac{2}{r} \left( P_{im} P_{jn} - \frac{1}{2} P_{ij} P_{mn} \right) \frac{d^2 Q_{mn}}{dt^2}, \quad (17)$$

where  $Q_{mn}$  is the reduced mass quadrupole moment

$$Q_{mn} = \text{STF} \left\{ \int \rho x^m x^n dV \right\} \quad (18)$$

and  $P_{ij} = \delta_{ij} - n_i n_j$  is the projection operator onto the plane transverse to the outgoing wave direction,  $n_i = x^i/r$ . For consistency with post-Newtonian accuracy, we must take into account the relativistic corrections up to the relative order  $(v/c)^2$ . This requires the time derivatives of the mass octupole, mass  $2^4$ -pole, current quadrupole and current octupole [2]. However we neglect these corrections since the gravitational wave amplitude is evaluated with quantities at each time step and small truncation errors above ‘Newtonian’ accuracy do not accumulate. With this accuracy, we can use  $I_{ij}$  defined by Eq.(16) in place of  $\ddot{Q}_{ij}$ . From Eq.(17), two polarizations are given by

$$\begin{aligned} h_+ &= \frac{1}{r} \left( I_{\hat{\theta}\hat{\theta}} - I_{\hat{\phi}\hat{\phi}} \right), \\ h_\times &= \frac{2}{r} I_{\hat{\theta}\hat{\phi}}, \end{aligned} \quad (19)$$

where  $I_{\hat{i}\hat{j}}$  is the quantity in the orthonormal basis

$$\begin{aligned} I_{\hat{\theta}\hat{\theta}} &= (I_{xx} \cos^2 \phi + I_{yy} \sin^2 \phi + 2I_{xy} \sin \phi \cos \phi) \cos^2 \theta \\ &\quad + I_{zz} \sin^2 \theta - 2(I_{xz} \cos \phi + I_{yz} \sin \phi) \sin \theta \cos \theta, \\ I_{\hat{\phi}\hat{\phi}} &= I_{xx} \sin^2 \phi + I_{yy} \cos^2 \phi - 2I_{xy} \sin \phi \cos \phi, \\ I_{\hat{\theta}\hat{\phi}} &= (I_{yy} - I_{xx}) \cos \theta \sin \phi \cos \phi + I_{xy} \cos \theta (\cos^2 \phi - \sin^2 \phi) \\ &\quad + I_{xz} \sin \theta \sin \phi - I_{yz} \sin \theta \cos \phi \end{aligned} \quad (20)$$

## 2.2. Numerical Methods

The equations are discretized by the finite difference method (FDM) with a uniform Cartesian grid. The evolution equations are integrated using van Leer’s scheme [4] with second-order accuracy in space. In order to make the scheme stable, a monotonicity condition, the so-called TVD (Total Variation Diminishing) limiter [5], is imposed on this scheme [6]. In order to achieve second-order

accuracy in time we adopt a two-step procedure as follows. To describe our code, we write Eqs.(1)–(3) as

$$\partial_t Q + \partial_j(Qv^j) = f(Q), \quad (21)$$

where  $Q$  is a 5-dimensional vector defined by

$$Q = (\rho, \rho w_i, \rho \varepsilon). \quad (22)$$

The elements of 5-vector  $f(Q)$  are given by the right hand sides of Eqs.(1)–(3). In order to obtain  $Q^{n+1} \equiv Q(t^n + \Delta t^n)$ , first we calculate the quantity  $Q^{n+\frac{1}{2}} \equiv Q(t^n + \Delta t^n/2)$  from  $Q^n$  as

$$Q^{n+\frac{1}{2}} = Q^n + F(Q^n) \frac{\Delta t^n}{2}, \quad (23)$$

and then calculate  $Q^{n+1}$  from  $Q^n$  and  $Q^{n+\frac{1}{2}}$  as

$$Q^{n+1} = Q^n + F(Q^{n+\frac{1}{2}}) \Delta t^n, \quad (24)$$

where  $F(Q)$  is the flux given by  $f(Q)$ .

In order to treat shock waves, we use a tensor artificial viscosity given by

$$p_{ij} = \begin{cases} \rho \ell^2 (\partial_k v^k) \text{STF} \{2 \partial_i v^j\} & \text{if } \partial_k v^k < 0, \\ 0 & \text{otherwise,} \end{cases} \quad (25)$$

where  $\ell$  is an appropriate number with units of length. The gas pressure  $p$  is replaced by  $P_{ij} = p\delta_{ij} + p_{ij}$ . The Poisson equations are solved using the MICCG (Modified Incomplete Cholesky-decomposition and Conjugate Gradient) method [7, 8, 9, 10, 11], which is fully vectorized using the hyperplane method proposed by Ushiro [11].

We have performed various tests for this code [12, 13], which include; (1) free transportation of a dust cube of a homogeneous or Gaussian density distribution, (2) a 1D Riemann shock tube, (3) a point explosion in the air, (4) local conservation of specific angular momentum for an axially symmetric collapse and (5) collapse of a homogeneous dust ellipsoid. Our code passed these tests with sufficiently good accuracy.

### 2.3. Newtonian Calculation

First we performed an extensive series of numerical calculations using Newtonian hydrodynamics including the radiation damping effects, where terms of order  $O(c^{-2})$  in Eqs.(5)–(8) are neglected while terms of order  $O(c^{-5})$  are kept to include the radiation damping effects.

### 2.3.1. Coalescence of Neutron Stars without Spin

We first consider initial data comprising of two neutron stars rotating rigidly around the center of mass. The binary system is assumed to be in rotational equilibrium at the initial time.

In order to obtain hydrostatic equilibrium models of close neutron star binaries, we set  $\partial_t = 0$ ,  $F_i^{\text{reac}} = 0$  and  $v^i = w_i$  in the Newtonian version of Eqs.(1)–(3). Here the gravitational radiation damping effects are neglected since a binary system evolves quasi-stationarily up to the onset of coalescence. Assuming the pressure  $p$  is given by  $p = K\rho^\gamma$  and the two stars are in a synchronized circular orbit around the center of mass  $(x_0, y_0, 0)$ , that is, the velocity is given by  $v^i = (-(y - y_0)\Omega, (x - x_0)\Omega, 0)$ , we have the equation that equilibrium models should satisfy:

$$\nabla \left[ \psi + H - \frac{1}{2} \{ (x - x_0)^2 + (y - y_0)^2 \} \Omega^2 \right] = 0, \quad (26)$$

where  $H$  is the enthalpy,

$$H = \frac{\gamma}{\gamma - 1} K \rho^{\gamma-1}. \quad (27)$$

A solution of Eq.(26) for each star is given by

$$\psi + H - \frac{1}{2} \{ (x - x_0)^2 + (y - y_0)^2 \} \Omega^2 = C_i \quad (\text{for } i=1, 2) \quad (28)$$

where  $C_1$  and  $C_2$  are different constants in general. Since the position of the center of mass can be set freely, we set  $y_0 = 0$ . Instead of setting  $x_0$ , however, we fix the positions  $x_1^s$  and  $x_2^s$  where the surface of each star intersects the  $x$ -axis between the stars;  $\rho(x_1^s, 0, 0) = \rho(x_2^s, 0, 0) = 0$ . In addition, we fix the center of each star  $x_1^c$  and  $x_2^c$  and the density there;  $\rho(x_1^c, 0, 0) = \rho_1^c$  and  $\rho(x_2^c, 0, 0) = \rho_2^c$ . A self-consistent solution is determined by an iterative method. First, setting the constants  $\gamma$  and  $K$  in the equation of state, we give an initial guess of the density distribution, usually as two spherical polytropes. Then we repeat the following steps until convergence:

- (1) The potential  $\psi$  is calculated as the solution of Eq.(10).
- (2)  $C_1$ ,  $C_2$ ,  $x_0$  and  $\Omega$  are determined from

$$\begin{aligned} \psi_1^c + H_1^c - \frac{1}{2} (x_1^c - x_0)^2 \Omega^2 &= C_1, \\ \psi_1^s - \frac{1}{2} (x_1^s - x_0)^2 \Omega^2 &= C_1, \\ \psi_2^c + H_2^c - \frac{1}{2} (x_2^c - x_0)^2 \Omega^2 &= C_2, \\ \psi_2^s - \frac{1}{2} (x_2^s - x_0)^2 \Omega^2 &= C_2; \end{aligned} \quad (29)$$

or explicitly

$$\begin{aligned} x_0 &= \frac{A_2\{(x_1^c)^2 - (x_1^s)^2\} - A_1\{(x_2^c)^2 - x_2^s\}^2}{2\{A_2(x_1^c - x_1^s) - A_1(x_2^c - x_2^s)\}}, \\ \Omega^2 &= \frac{A_1}{(x_1^c - x_1^s)(x_1^c + x_1^s - 2x_0)}, \\ C_i &= \psi_i^s - \frac{1}{2}(x_i^s - x_0)^2\Omega^2, \end{aligned} \quad (30)$$

where  $\psi_a \equiv \psi(x_a, 0, 0)$ ,  $H_a \equiv H(x_a, 0, 0)$  and  $A_i \equiv \psi_i^c - \psi_i^s + H_i^c$ .

(3) Using these values, we determine a new density distribution from

$$H = \frac{\gamma}{\gamma - 1} K \rho^{\gamma-1} = C_i - \psi + \frac{1}{2}\{(x - x_0)^2 + y^2\}\Omega^2. \quad (31)$$

Here we use the constant  $C_1$  for  $x > x_0$  and  $C_2$  for  $x < x_0$ .

To be more realistic, we consider an infalling velocity due to the gravitational radiation. Assuming that the two stars are point masses with separation  $\ell$  in a circular orbit,  $\ell$  decreases at a rate

$$\partial_t \ell = - \frac{64m_1m_2(m_1 + m_2)}{5\ell^3}. \quad (32)$$

We therefore add the infalling velocity given by this equation to the initial stars.

We typically use a  $141 \times 141 \times 131$  grid. We assume reflection symmetry with respect to the  $z = 0$  plane and consider the region of  $z \geq 0$  only, since the system becomes rather flat and therefore needs a finer grid in the  $z$ -direction. Calculations were performed on a HITAC S820/80 supercomputer at the National Laboratory for High Energy Physics (KEK). Each calculation requires approximately 900Mbytes of memory. A typical CPU time required is 100–200 hours for up to 50,000–90,000 time steps, which corresponds to an event lasting 4–8 milliseconds.

Here we show the results for neutron stars of  $1.5M_\odot + 1.5M_\odot$  (EQSP2). Figure 1 shows the evolution of the density and the velocity on the  $x$ - $y$  plane, where, at the initial time, the radius of each star is 8.8km, the separation between stars  $\ell_0$  is 27km, the angular velocity  $\Omega$  is  $4.1 \times 10^3 \text{sec}^{-1}$ . In each figure only the central part is represented, while the computational grid covers  $[-47\text{km}, 47\text{km}]$  in the  $x$  and  $y$  directions and  $[0\text{km}, 49\text{km}]$  in the  $z$  direction. Figure 2 shows the emitted energy  $L$  and the central density  $\rho_c$  as functions of time. The gravitational radiation takes the angular momentum away from the system; in fact,  $a/m \equiv J_t/(GM^2/c^3) = 0.64$  at first and  $a/m = 0.38$  finally. Since the greatest part of the matter is within the Schwarzschild radius  $r = GM_t/c^2$  as shown in Fig.1i, the final destiny of the system must be a slowly rotating black hole. The energy emitted in gravitational radiation is

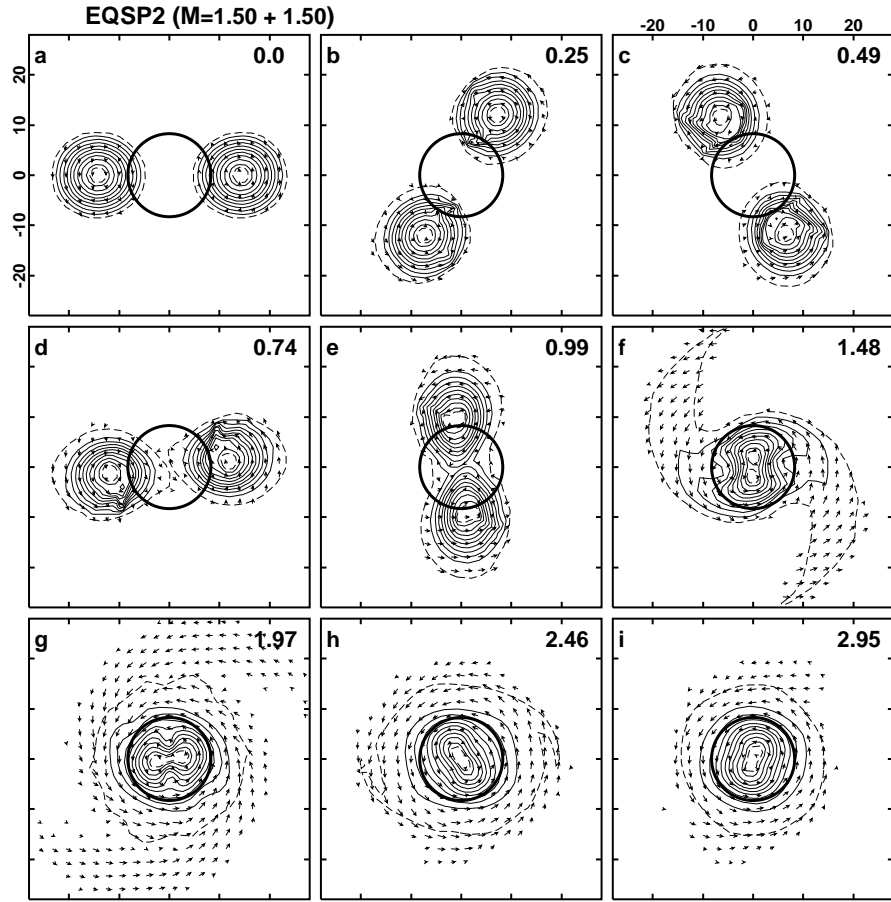


Fig. 1. — Density and velocity on the  $x-y$  plane for EQSP2. The time in units of milliseconds is shown. Solid lines are drawn in steps of a tenth of the maximum density and the inner and the outer dashed lines indicate 19/20 and 1/20 of maximum density. Arrows indicate the velocity vectors of the matter. A fat line shows a circle of radius  $2GM_t/c^2$  to show the size of a spherical black hole for comparison.



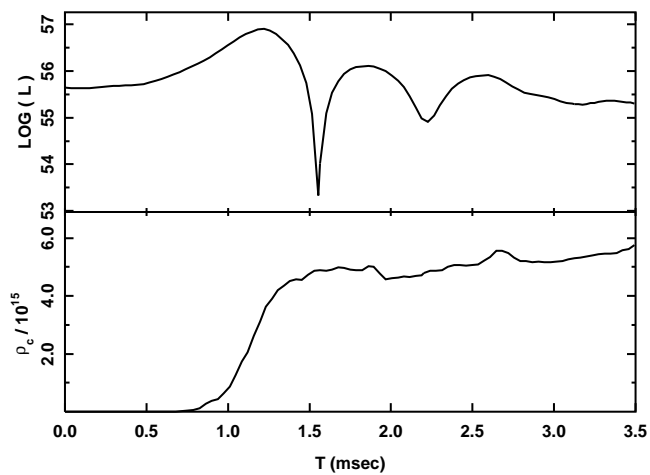


Fig. 2. — Luminosity (in units of erg/sec) and central density (in units of  $\text{g}/\text{cm}^3$ ) as functions of time (in units of millisecond) for EQSP2.

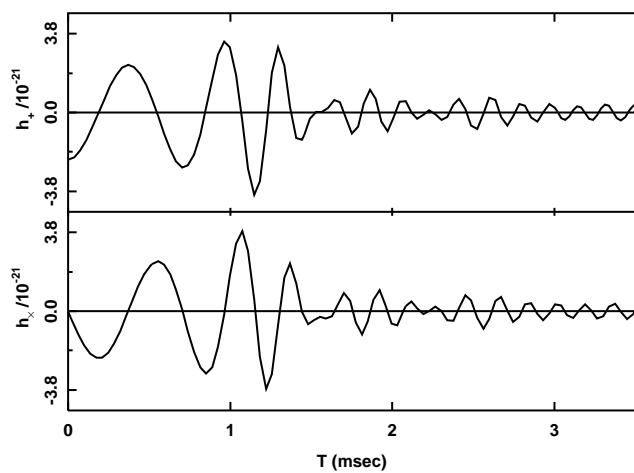


Fig. 3. — Wave forms of  $h_+$  and  $h_x$  observed on the  $z$ -axis at 10Mpc for EQSP2.

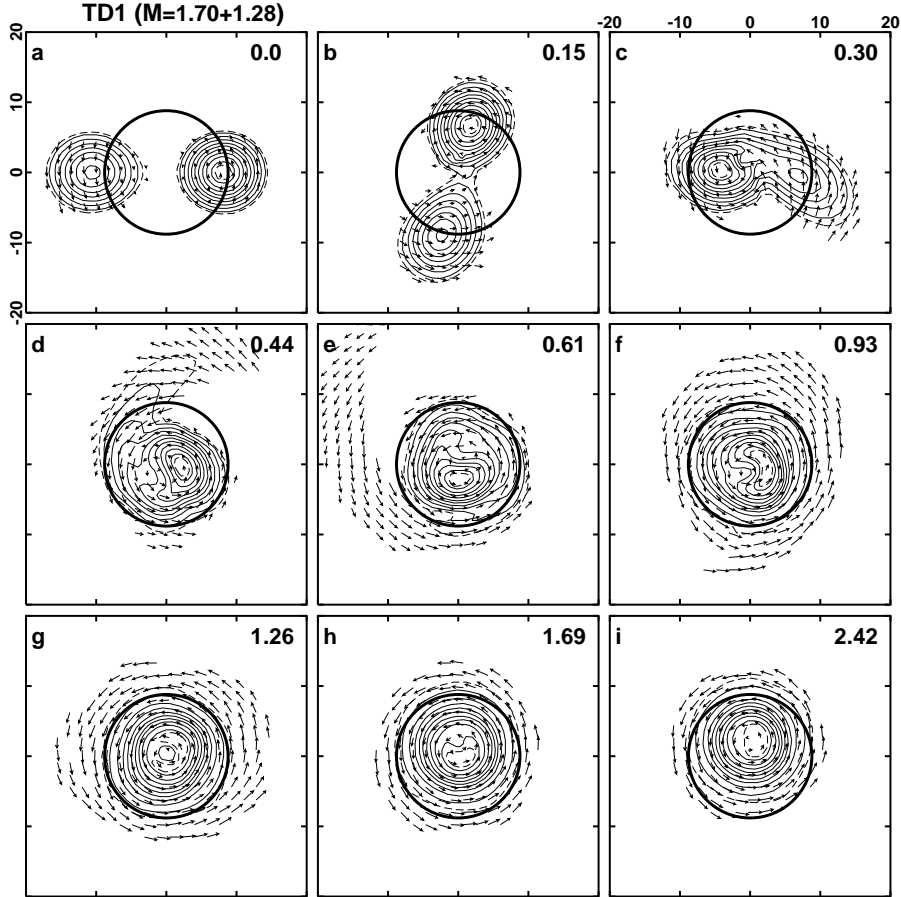


Fig. 4. — Density and velocity on the  $x$ - $y$  plane for TD1.

$1.6 \times 10^{53}$ erg, which is 3% of the total rest mass. This means that the efficiency of gravitational radiation is 30 times larger than the results for axisymmetric simulations by Smarr [14] or Stark and Piran [15].

Figure 3 shows the wave forms  $h_+$  and  $h_\times$  observed along the  $z$ -axis, which are given by

$$\begin{aligned} h_+ &= \frac{1}{r} (I_{xx} - I_{yy}), \\ h_\times &= \frac{2}{r} I_{xy}, \end{aligned} \quad (33)$$

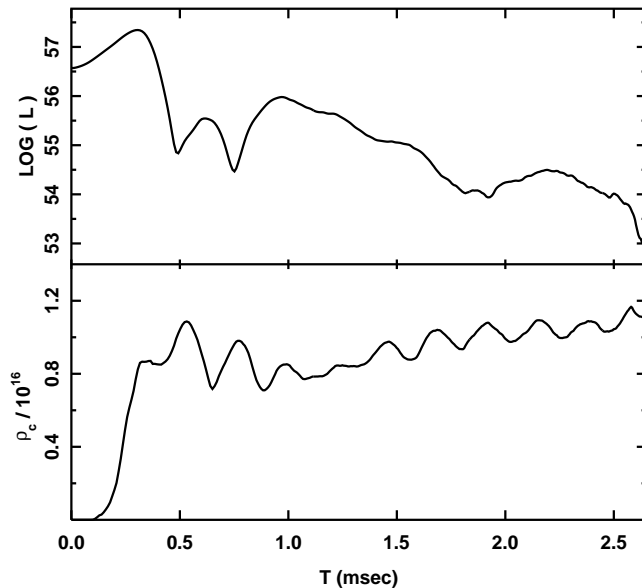


Fig. 5. — Luminosity (in units of erg/sec) and central density (in units of  $\text{g/cm}^3$ ) as functions of time (in units of millisecond) for TD1.

where  $r$  is the distance between the event and the observer. If the event occurs at 10Mpc from the earth, the maximum amplitude of  $h$  is  $4.0 \times 10^{-21}$ .

Figures 4 and 5 is the same as Figs.1 and 2, but for the model TD1, where the masses of stars are  $1.70M_\odot$  and  $1.28M_\odot$ , the radii are 7km and 8km,  $\Omega = 7.9 \times 10^3 \text{sec}^{-1}$  and  $J_t = 5.1GM_\odot^2/c$ .

### 2.3.2. Coalescence of Neutron Stars with Spin

In the previous subsection, we place two neutron stars in a rotational equilibrium state with rigid rotation around the center of mass as the initial condition. However, in the absence of the viscosity, the circulation  $\Gamma$  of the system should be conserved:

$$\Gamma = \int_S (\nabla \times \mathbf{v}) \cdot d\mathbf{S} = \oint_{\partial S} \mathbf{v} \cdot d\boldsymbol{\ell} = \text{const.} \quad (34)$$

If the stars are assumed to rotate rigidly around the center of mass at first, the circulation in the  $z = \text{constant}$  plane is  $2\Omega_0 S$ , where  $\Omega_0$  and  $S$  are the initial angular velocity and the area of the cross section of the stars, respectively. While two stars approach each other, the area of the cross section of the stars does not change so much, but the angular velocity  $\Omega$  becomes much larger than  $\Omega_0$  as  $\Omega \propto (\text{separation})^{3/2}$ . Then, the stars must have spin with the angular

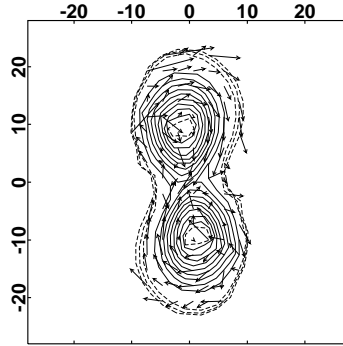


Fig. 6. — The same as Fig.1e. The arrows show the velocity relative to the center of each star, which shows the spin retrograde to the orbital motion.

velocity  $-\Omega$  to conserve the circulation. This is illustrated in Fig.6. It is the same figure as Fig.1e, but the arrows show the velocity relative to the center of each star.

To take into account this effect, we consider two neutron stars rotating around the center of mass but also having spin angular velocity retrograde to the orbital motion [16]. In this case, we don't know how to determine an equilibrium model because this is a similar problem to determine the Dedekind configuration [17]. As for an axisymmetric rotating star, however, we can obtain the equilibrium configurations. We here consider axisymmetric rotation stars as the initial condition for each spinning star. The equilibrium configuration for a spinning star is determined by Eq.(29) with  $\psi_i$  and  $\Omega$  being the gravitational potential of each star alone and the spin angular momentum, respectively, as well as  $x_0 = x_i^c$ . Then we assume that the orbital velocity of each star is the Keplerian one,  $\Omega_K = \sqrt{G(m_1 + m_2)/\ell_0^3}$ , where  $m_1$ ,  $m_2$  and  $\ell_0$  are mass of each star and the separation of each star, and that  $\Omega = -\Omega_K$ . This initial condition is consistent if the tidal force is much smaller than the self-gravity.

Initially the orbital velocity  $\mathbf{v}_K$  is given by

$$v_K^x = -y\Omega_K, \quad v_K^y = x\Omega_K \quad (35)$$

and the spin velocity  $\mathbf{v}_s$  is given by

$$v_s^x = y\Omega_K$$

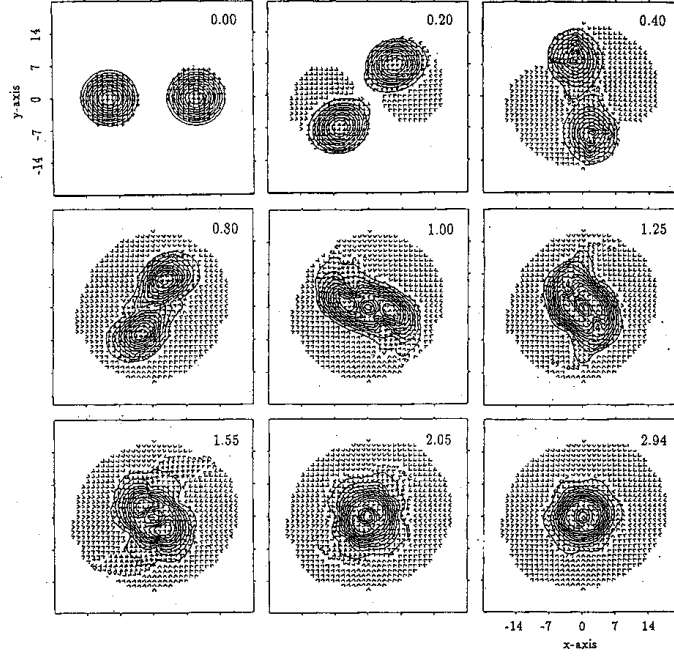


Fig. 7. — Density and velocity on the  $x$ - $y$  plane for SPIN1.

$$v_s^y = \begin{cases} -\left(x - \frac{\ell_0}{2}\right) \Omega_K & (x > 0) \\ -\left(x + \frac{\ell_0}{2}\right) \Omega_K & (x < 0). \end{cases} \quad (36)$$

Since  $v_K^x + v_s^x = 0$  in the inertial frame, the velocity vector points to only  $y$ -direction. Figure 7 shows the evolution of the density and the velocity on the  $x$ - $y$  plane, where, at the initial time, the mass and the radius of each star are  $1.40M_\odot$  and 9km, the separation between stars  $\ell_0$  is 27km. The evolution sequence is almost the same as EQSP2 up to the onset of coalescence. After coalescence starts, however, the evolution of the system is quite different; there is no spiral arm in the outer region and the configuration becomes a nearly axially symmetric disk soon. This is because the velocity in the outer region is smaller on account of the spin retrograde to the orbital motion and the centrifugal force is weaker than EQSP2. The stars are gradually coalescing because the centrifugal force is enhanced in the inner region, and the double

core structure is kept for a long time. The radiation reaction makes the double cores merge at last.

## 2.4. Post-Newtonian Calculation

Now we show results of a (1+2.5) post-Newtonian calculation we performed in order to study general relativistic effects. We performed also a Newtonian calculation with the same initial data for comparison. The initial data includes two spherical neutron stars, namely two relativistic polytropes with  $\gamma = 2$  whose surfaces just touch each other. The mass and the radius of each star is  $0.62M_{\odot}$  and 15km, respectively. The two stars are rotating around the center of mass with angular velocity  $\Omega = 2.0 \times 10^3 \text{sec}^{-1}$ . The total angular momentum,  $J_t$ , of the system is  $1.6GM_{\odot}^2/c$ .

Figure 8 shows the evolution of the density and the velocity on the  $x$ - $y$  plane and Fig.9 shows the emitted energy  $L$  and the central density  $\rho_c$  as functions of time. The result of the post-Newtonian(PN) calculation is shown on the right of Fig.8 and as solid lines in Fig.9, while the result of the Newtonian(N) calculation is on the left and as dashed lines. In PN, coalescence begins more rapidly since general relativity effectively increases the gravitational force. Then a strong shock appears which makes the matter reexpand, and a radial oscillation with large amplitude is excited. The coalescence-expansion oscillation lasts longer in the PN case than in the N case. As a result the total energy emitted in the gravitational radiation increases in comparison with the N case;  $3.4 \times 10^{50}$ erg in PN and  $2.2 \times 10^{50}$ erg in N up to 8.6msec. Figure 10 shows the wave form observed along the  $z$ -axis, where solid lines are for PN and dashed lines are for N. Although  $h$  is damped faster in N, the maximum amplitudes are almost the same. The appearance of the strong shock in the PN calculation has little effect on the wave form.

The difference between PN and N is caused principally by the strong shock which appears in the initial stage. Thus if the initial data consists of two stars in rotational equilibrium and coalescence proceeds more slowly, the difference between PN and N may be less pronounced. However we do not consider the red-shift effect and excitation of the quasi-normal modes of the resulting black hole or neutron star, which may be essential in the gravitational radiation [15, 18]. To complete the program of studying a final destiny of a coalescing binary system and computing emission of gravitational waves in such a event, we should solve a full set of the Einstein equation.

## 3. GENERAL RELATIVISTIC SIMULATIONS

In this section, we discuss recent developments of our fully general relativistic code for numerical calculation of *the last three milliseconds* of coalescing binary neutron stars.

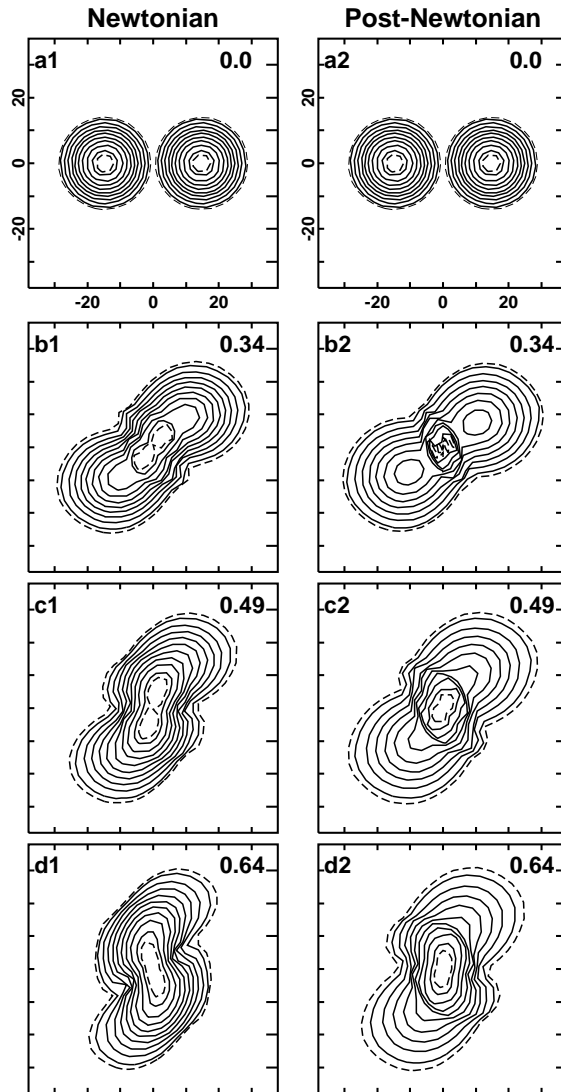
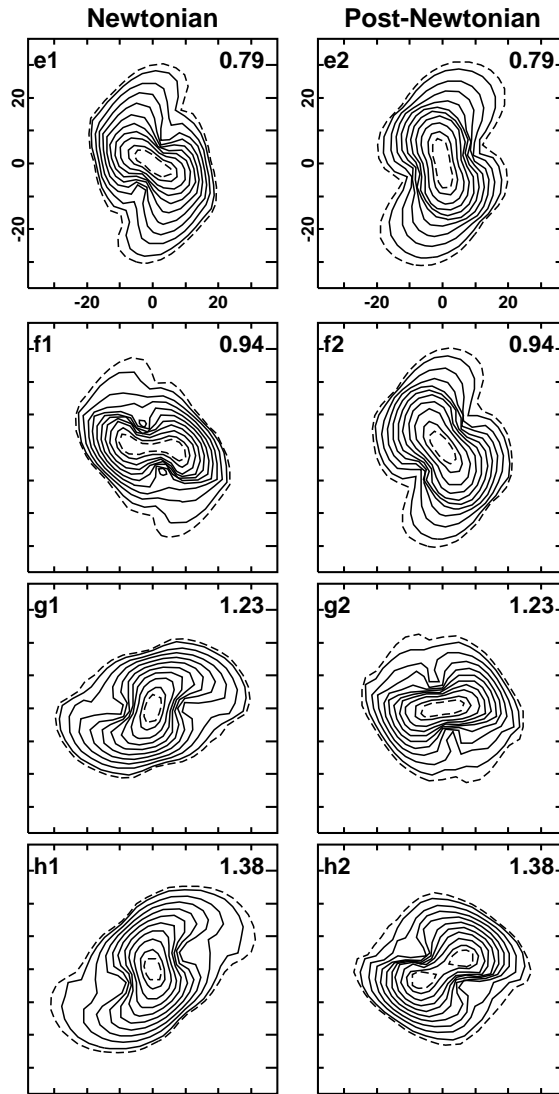
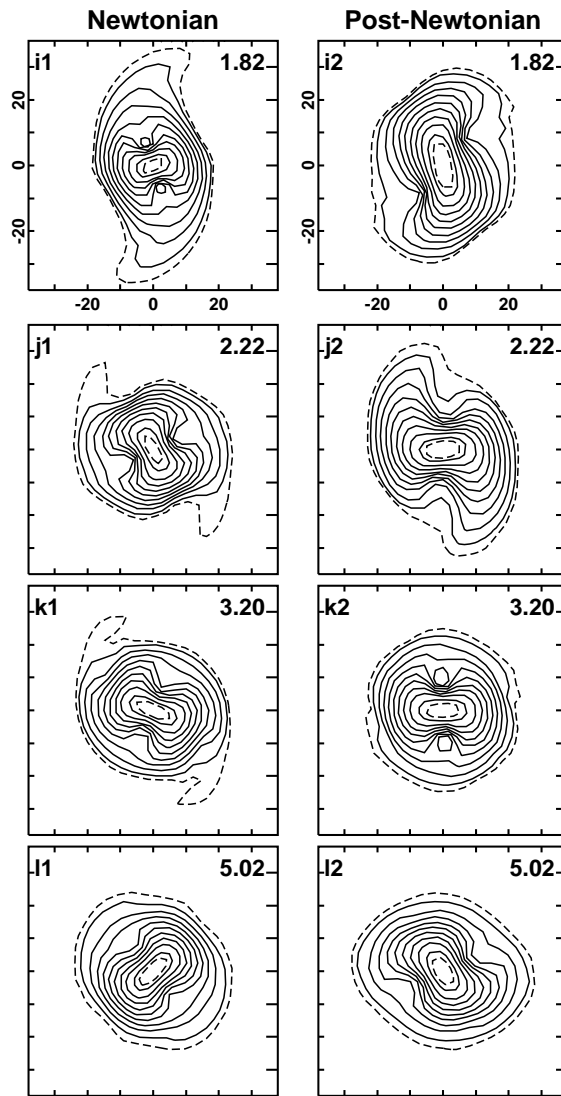


Fig. 8. — Density on the  $x-y$  plane. The left and right figures are for the Newtonian(N) and post-Newtonian(PN) calculations, respectively. Notations are the same as for Fig.1.







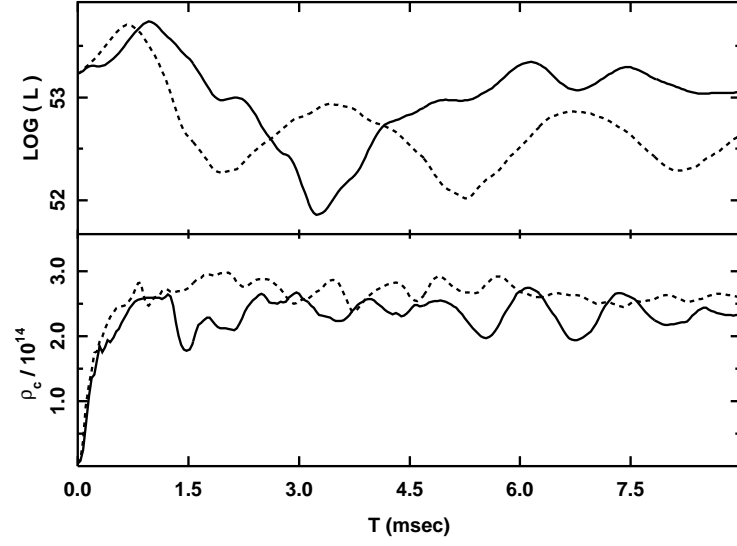


Fig. 9. — Luminosity (in units of erg/sec) and central density (in units of  $\text{g}/\text{cm}^3$ ) as functions of time (in units of millisecond). The solid and dashed lines are for PN and N, respectively.

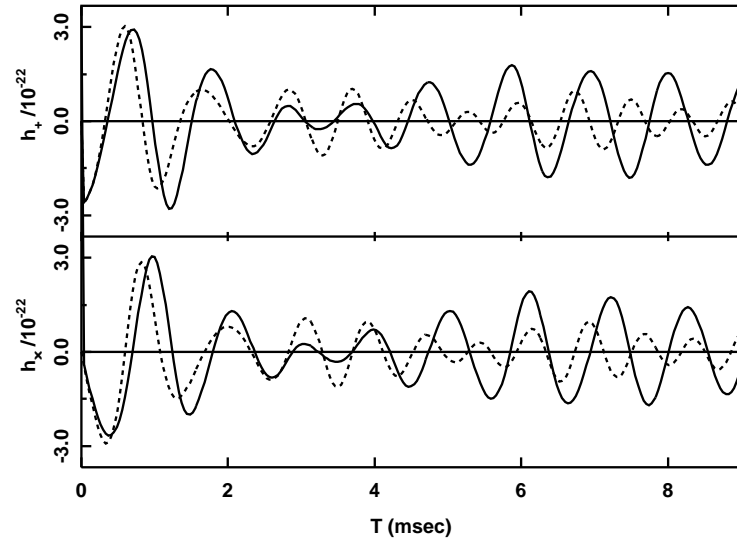


Fig. 10. — Wave forms of  $h_+$  and  $h_x$  observed on the  $z$ -axis at 10Mpc. The solid and dashed lines are for PN and N, respectively.

### 3.1. Basic Equations

#### 3.1.1. Initial Value Equations

In the (3+1)-formalism of the Einstein equation, the line element takes the form

$$ds^2 = -\alpha^2 dt^2 + \gamma_{ij}(dx^i + \beta^i dt)(dx^j + \beta^j dt), \quad (37)$$

where  $\alpha$ ,  $\beta^i$  and  $\gamma_{ij}$  are the lapse function, the shift vector and the intrinsic metric of 3-space, respectively. The initial data should satisfy the constraint equations

$$R + K^2 - K_{ij}K^{ij} = 16\pi\rho_H, \quad (38)$$

$$D_j (K^j_i - \delta^j_i K) = 8\pi J_i, \quad (39)$$

where  $R$  is the 3-dimensional Ricci scalar curvature,  $K_{ij}$  is the extrinsic curvature,  $K$  is its trace and the symbol  $D_i$  denotes the covariant derivative with respect to  $\gamma_{ij}$ . The quantities  $\rho_H$  and  $J_i$  are, respectively, the energy density and the momentum density of the matter measured by the normal line observer. The relation of these quantities to the stress-energy tensor is given by Eq.(55) below.

Now we assume that on the Cauchy slice the trace  $K = 0$  and  $\gamma_{ij}$  is conformally flat, that is,

$$\gamma_{ij} = \phi^4 \tilde{\gamma}_{ij}, \quad (40)$$

where  $\tilde{\gamma}_{ij}$  is the flat metric. Defining the conformal transformation as

$$\begin{aligned} \tilde{K}_{ij} &\equiv \phi^2 K_{ij}, & \tilde{K}_i^j &\equiv \phi^6 K_i^j & \tilde{K}^{ij} &\equiv \phi^{10} K^{ij} \\ \rho_B &\equiv \phi^6 \rho_H & \text{and } \tilde{J}_i &\equiv \phi^6 J_i, \end{aligned} \quad (41)$$

Eq.(39) can be expressed as

$$\tilde{D}_j \tilde{K}^j_i = 8\pi \tilde{J}_i, \quad (42)$$

where  $\tilde{D}_i$  is the covariant derivative with respect to  $\tilde{\gamma}_{ij}$  [19]. The traceless extrinsic curvature can be decomposed with the transverse traceless part  $\tilde{K}_{ij}^{\text{TT}}$  and the longitudinal traceless part  $(LW)_{ij}$  [20];

$$\tilde{K}_{ij} = \tilde{K}_{ij}^{\text{TT}} + (LW)_{ij}, \quad (43)$$

where

$$(LW)_{ij} = \tilde{D}_i W_j + \tilde{D}_j W_i - \frac{2}{3} \tilde{\gamma}_{ij} \tilde{D}^\ell W_\ell. \quad (44)$$

Assuming  $\tilde{K}_{ij}^{\text{TT}} = 0$ , Eq.(42) is reduced to

$$\tilde{\Delta} W_i + \frac{1}{3} \tilde{D}_i \tilde{D}^j W_j = 8\pi \tilde{J}_i, \quad (45)$$

where  $\tilde{\Delta} \equiv \tilde{D}^i \tilde{D}_i$ . Equation (45) is the coupled elliptic equation but, by defining

$$\chi \equiv \tilde{D}_i W^i, \quad (46)$$

it can be decoupled into

$$\tilde{\Delta} \chi = 6\pi \tilde{D}_i \tilde{J}^i \quad (47)$$

and

$$\tilde{\Delta} W_i = 8\pi \tilde{J}_i - \frac{1}{3} \tilde{D}_i \chi. \quad (48)$$

The boundary conditions for  $\chi$  and  $W_i$  are

$$\chi = O\left(\frac{1}{r^4}\right) \quad (49)$$

and

$$W_i = \frac{\epsilon_{ijk} x^j M^k}{r^3} + O\left(\frac{1}{r^3}\right), \quad (50)$$

where  $M^k$  is a constant related to the angular momentum of the system.

The conformal transformation of the scalar curvature is

$$R = \phi^{-4} \tilde{R} - 8\phi^{-5} \tilde{\Delta} \phi, \quad (51)$$

where  $\tilde{R}$  is the scalar curvature with respect to  $\tilde{\gamma}_{ij}$ . Since  $\tilde{R} = 0$  for a conformally flat metric, Eq.(38) is reduced to

$$\tilde{\Delta} \phi = -2\pi \phi^{-1} \rho_B - \frac{1}{8} \phi^{-7} \tilde{K}_{ij} \tilde{K}^{ij}. \quad (52)$$

The boundary condition for  $\phi$  is

$$\phi = 1 + \frac{M_G}{2r} + O\left(\frac{1}{r^3}\right), \quad (53)$$

where  $M_G$  is the gravitational mass of the system.

### 3.1.2. Relativistic Hydrodynamics

We assume the perfect fluid stress-energy tensor, which is given by

$$T_{\mu\nu} = (\rho + \rho\varepsilon + p)u_\mu u_\nu + pg_{\mu\nu}, \quad (54)$$

where  $\rho$ ,  $\varepsilon$  and  $p$  are the proper mass density, the specific internal energy and the pressure, respectively, and  $u_\mu$  is the four-velocity of the fluid. The energy density  $\rho_H$ , the momentum density  $J_i$  and the stress tensor  $S_{ij}$  of the matter measured by the normal line observer are, respectively, given by

$$\rho_H \equiv n^\mu n^\nu T_{\mu\nu}, \quad J_i \equiv -h_i^\mu n^\nu T_{\mu\nu} \quad \text{and} \quad S_{ij} \equiv h_i^\mu h_j^\nu T_{\mu\nu}, \quad (55)$$

where  $n_\mu$  is the unit timelike four-vector normal to the spacelike hypersurface and  $h_{\mu\nu}$  is the projection tensor into the hypersurface defined by

$$h_{\mu\nu} = g_{\mu\nu} + n_\mu n_\nu. \quad (56)$$

The relativistic hydrodynamics equations are obtained from the conservation of baryon number,  $\nabla_\mu(\rho u^\mu)$ , and the energy-momentum conservation law,  $\nabla_\nu T_\mu{}^\nu$ . In order to obtain equations similar to the Newtonian hydrodynamics equations, we define  $\rho_N$  and  $u_i^N$  as

$$\rho_N \equiv \sqrt{\gamma} \alpha u^0 \rho \quad \text{and} \quad u_i^N = \frac{J_i}{\alpha u^0 \rho}, \quad (57)$$

respectively, where  $\gamma = \det(\gamma_{ij})$ . Then the equation for the conservation of baryon number takes the form

$$\partial_t \rho_N + \partial_\ell (\rho_N V^\ell) = 0, \quad (58)$$

where

$$V^\ell = \frac{u^\ell}{u^0} = \frac{\alpha J^\ell}{p + \rho_H}. \quad (59)$$

The equation for momentum conservation is

$$\begin{aligned} \partial_t (\rho_N u_i^N) + \partial_\ell (\rho_N u_i^N V^\ell) &= -\sqrt{\gamma} \alpha \partial_i p - \sqrt{\gamma} (p + \rho_H) \partial_i \alpha \\ &\quad - \frac{\sqrt{\gamma} \alpha J^k J^\ell}{2(p + \rho_H)} \partial_i \gamma_{k\ell} + \sqrt{\gamma} J_\ell \partial_i \beta^\ell. \end{aligned} \quad (60)$$

The equation for internal energy conservation becomes

$$\partial_t (\rho_N \varepsilon) + \partial_\ell (\rho_N \varepsilon V^\ell) = -p \frac{1}{\alpha \sqrt{\gamma}} \partial_\nu (\sqrt{\gamma} \alpha u^\nu). \quad (61)$$

To complete hydrodynamics equations, we need an equation of state,

$$p = p(\varepsilon, \rho). \quad (62)$$

Equations (58)–(61), whose structure is the same as Eqs.(1)–(3), can be solved using the post-Newtonian hydrodynamics code described the previous section.

### 3.1.3. Time Evolution of the Extrinsic Curvature

The evolution equation for the extrinsic curvature takes the form

$$\partial_t K_{ij} - \partial_\ell (K_{ij} \beta^\ell) = (SK)_{ij}^{\text{main}} + (SK)_{ij}^{\text{NL}} + (SK)_{ij}^\beta, \quad (63)$$

where

$$(SK)_{ij}^{\text{main}} = \alpha \left\{ R_{ij} - 8\pi \left[ S_{ij} + \frac{1}{2} \gamma_{ij} (\rho_H - S^\ell{}_\ell) \right] \right\} - D_i D_j \alpha \quad (64)$$

$$(SK)_{ij}^{\text{NL}} = \alpha (K K_{ij} - 2K_{i\ell} K^\ell{}_j), \quad (65)$$

$$(SK)_{ij}^\beta = K_{mi} \partial_j \beta^m + K_{mj} \partial_i \beta^m - K_{ij} \partial_m \beta^m, \quad (66)$$

and  $R_{ij}$  is the 3-dimensional Ricci tensor. Equation (63) can be solved in the same way as the hydrodynamics equations with the velocity  $-\beta^\ell$  instead of  $V^\ell$ .

### 3.1.4. Time Slicing

Defining the conformal factor  $\phi$  as

$$\phi \equiv (\det(\gamma_{ij}))^{\frac{1}{12}}, \quad (67)$$

we use the lapse function  $\alpha$  given by

$$\alpha = \exp \left[ -2 \left( (\phi - 1) + \frac{(\phi - 1)^3}{3} + \frac{(\phi - 1)^5}{5} \right) \right]. \quad (68)$$

Shibata and Nakamura[21] called this time slicing as the conformal time slicing because  $\alpha$  is determined by the conformal factor  $\phi$ . In the conformal time slicing, the space outside the central matter quickly approaches the Schwarzschild metric. Detailed discussion on the nature of the conformal time slicing is given in the reference [21]. The equation for the conformal factor  $\phi$  is obtained from the Hamiltonian constraint equations,

$$\tilde{\Delta}\phi = -\frac{\phi^5}{8} (16\pi\rho_H + K_{ij}K^{ij} - K^2 - \phi^{-4}R), \quad (69)$$

where  $\tilde{\Delta}$  is the Laplacian with respect to

$$\tilde{\gamma}_{ij} = \phi^{-4}\gamma_{ij}. \quad (70)$$

Note that  $\tilde{\gamma}_{ij}$  is *not* the flat-space metric for  $t \neq 0$ .

### 3.1.5. Spatial Coordinates

Here we define conformal transformation, different from Eq.(41), as

$$\begin{aligned} \tilde{K}_{ij} &\equiv \phi^{-4}K_{ij}, & \tilde{K}_i^j &\equiv K_i^j, & \tilde{K} &\equiv K, \\ \tilde{\beta}_i &\equiv \phi^{-4}\beta_i & \text{and } \tilde{\beta}^i &\equiv \beta^i, \end{aligned} \quad (71)$$

and the equation for metric thereby becomes

$$\begin{aligned} \partial_t \tilde{\gamma}_{ij} &= \left( \tilde{D}_i \tilde{\beta}_j + \tilde{D}_j \tilde{\beta}_i - \frac{2}{3} \tilde{\gamma}_{ij} \tilde{D}_\ell \tilde{\beta}^\ell \right) - 2\alpha \left( \tilde{K}_{ij} - \frac{1}{3} \tilde{\gamma}_{ij} \tilde{K} \right) \\ &\equiv A_{ij}^T, \end{aligned} \quad (72)$$

where  $\tilde{D}_i$  denotes the covariant derivative with respect to  $\tilde{\gamma}_{ij}$  defined by Eq.(70). Now we demand the divergence with respect to the flat-space metric of the right hand side of Eq.(72) to vanish,

$$\partial_i A_{ij}^T = 0, \quad (73)$$

which is reduced to the equation for the shift vector  $\beta^i$ ,

$$\nabla^2 \beta^i + \frac{1}{3} \partial_i (\partial_\ell \beta^\ell) =$$

$$\begin{aligned} & \partial_j \left[ 2\alpha \left( \tilde{K}_{ij} - \frac{1}{3} \tilde{\gamma}_{ij} K \right) \right] \\ & - \partial_j \left[ \hat{\gamma}_{j\ell} \partial_i \beta^\ell + \hat{\gamma}_{i\ell} \partial_j \beta^\ell - \frac{2}{3} \hat{\gamma}_{ij} \partial_\ell \beta^\ell + \beta^\ell \partial_\ell \hat{\gamma}_{ij} \right], \end{aligned} \quad (74)$$

where  $\nabla^2$  is the simple flat-space Laplacian and  $\hat{\gamma}_{ij} = \tilde{\gamma}_{ij} - \delta_{ij}$ . Equation (74) is similar to Eq.(45) while  $\beta^i$  appears in the right hand side, too.

If we demand

$$\tilde{D}^j A_{ij}^T = 0, \quad (75)$$

instead of Eq.(73), we have the minimal distortion condition proposed by York and Smarr [22]. In this sense, we call Eq.(73) the pseudo-minimal distortion condition.

### 3.2. Numerical Methods

We use Cartesian  $(x, y, z)$  isotropic coordinates for relativistic simulation, too. The hydrodynamics equations, Eqs.(58)–(61), and the evolution equations for the extrinsic curvature, Eq.(63), and the 3-metric, Eq.(72), are solved through the same scheme as in the Newtonian simulation. The elliptic equations are solved through the MICCG method. The equation for the conformal factor in the initial hypersurface, Eq.(52), can be reduced to

$$\nabla^2 \phi = 4\pi \rho_1(\phi), \quad (76)$$

since the initial hypersurface is conformally flat ( $\tilde{\Delta} = \nabla^2$ ). The source term  $\rho_1(\phi)$  is a non-linear function of  $\phi$ . This equation is solved by an iterative method: The following iteration is repeated until convergence,

$$\phi^{(I+1)} = (\nabla^2)^{-1} \left[ 4\pi \rho_1 \left( \phi^{(I)} \right) \right] \quad (\text{for } I = 1, 2, \dots). \quad (77)$$

Equations (69) and (74) for  $t > 0$  are also non-linear or coupled elliptic equations, which can be written as

$$\nabla^2 \phi = 4\pi \rho_2(\phi), \quad (78)$$

$$\nabla^2 \chi = 3\pi \partial_i \left( \rho_3^i(\beta) \right) \quad (79)$$

and

$$\nabla^2 \beta^i = -\frac{1}{3} \partial_i \chi + 4\pi \rho_3^i(\beta), \quad (80)$$

where  $\chi \equiv \partial_\ell \beta^\ell$ . The cost of finding self-consistent solutions for Eqs.(78)–(80) at each time step is very expensive and hence we use the values at the previous time step for  $\phi$  and  $\beta^i$  in the source terms  $\rho_2$  and  $\rho_3$ . The accuracy of solutions by this method seems to be sufficient to examine the global behavior of the numerical schemes and the coordinate conditions. The method should be improved in a future version.

Although any equation of state can be used, for the present test calculation, we use a simple equations state Eq.(4) with  $\gamma = 2$  to express a hard equation of state for a neutron star.

### 3.3. Numerical Results

Now we show results of test calculations. Here we use units of

$$M = M_{\odot}, \quad L = \frac{GM_{\odot}}{c^2} \quad \text{and} \quad T = \frac{GM_{\odot}}{c^3}. \quad (81)$$

In the following test calculations, we use a  $80 \times 80 \times 80$  grid covering  $[-40, 40]$  in each direction.

#### 3.3.1. Spherically Symmetric Dust Collapse

In the conformal time slicing given by Eq.(68), the time-variable parts of  $\tilde{\gamma}_{ij}$  can be considered as gravitational radiation parts, since the space outside the central matter approaches the Schwarzschild metric quickly [21]. Thus the total energy of the gravitational waves is given by

$$E_{\text{GW}} = \int dt \int_{r \rightarrow \infty} d\Omega \frac{r^2}{32\pi} (A_{ij}^{\text{TT}})^2, \quad (82)$$

where  $A_{ij}^{\text{TT}}$  is the transverse-traceless part of the time derivative of  $\tilde{\gamma}_{ij}$ ,

$$A_{ij}^{\text{TT}} = (\partial_t \tilde{\gamma}_{ij})^{\text{TT}} \quad (83)$$

and the time derivative of  $\tilde{\gamma}_{ij}$  is given by Eq.(72). Now we define the ‘‘energy density of the gravitational waves’’, although it cannot be defined locally, as

$$\rho_{\text{GW}} = \frac{1}{32\pi} (A_{ij}^{\text{TT}})^2 = \frac{1}{32\pi} (A^{\text{TT}})_{ij} (A^{\text{TT}})^{ij}. \quad (84)$$

In order to examine whether  $A_{ij}^{\text{TT}}$  shows the gravitational waves’ degree of freedom, we performed calculation of collapse of a spherically symmetric dust star of mass  $M$ . Figure 11 shows the mass density  $\rho_N$  and the ‘‘energy density of the gravitational waves’’  $r^2 \rho_{\text{GW}}$ . Although  $r^2 \rho_{\text{GW}}$  has a non-zero value near the center, it does not propagate outward. Since the meaning of ‘‘transverse-traceless’’ is clear only in the asymptotically flat region, the results is consistent with the idea that  $A_{ij}^{\text{TT}}$  represents the gravitational waves. The total energy of the gravitational waves  $E_{\text{GW}}$  is  $\sim 10^{-7}M$  at  $t = 30M$  observed at  $r = 20M$ . This value is essentially zero within numerical errors.

#### 3.3.2. Formation of a Rotating Black Hole

Stark and Piran [15] performed axially symmetric simulations for formation of a black hole and directly computed their gravitational radiation emission. For comparison with their results, we set similar initial conditions, although our coordinate condition is different from theirs. We use a simple equation of state, Eq.(4), which is the same as Stark and Piran. We place a spherically symmetric star of  $\gamma = 2$  polytrope of mass  $1M_{\odot}$  with internal energy necessary for Newtonian equilibrium. The rotation velocity with constant  $\Omega$  is added to



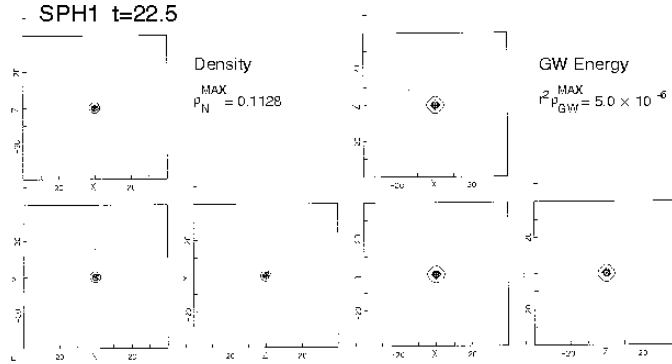


Fig. 11. — Mass density  $\rho_N$  (left) and “energy density of the gravitational waves”  $r^2 \rho_{GW}$  (right) on the  $x$ - $y$ ,  $y$ - $z$  and  $x$ - $z$  planes for a spherically symmetric dust collapse. The time in units of  $M_\odot$ , and the maximum value of density in units of  $M_\odot^{-2}$  are shown.

this system. We performed four simulations, ROT1, ROT2, ROT3 and ROT4, each of which is characterized by the initial value of  $a/M_g$ , where  $a$  is the angular momentum per unit gravitational mass  $M_g$ . The value of  $a/M_g$  is 0.3, 0.5, 0.8 and 1.0, respectively.

Figure 12 shows the evolution of density distribution of ROT4. It represents that the centrifugal force prevents the star from collapse in the direction perpendicular to the rotation axis and the star becomes an oblate spheroid. The “energy of gravitational waves” is shown in Fig.13. A pattern almost axially symmetric with a few peaks appears on the  $x$ - $y$  plane. Deviation from axial symmetry is caused by coarseness of our Cartesian grid. The wave pattern on  $x$ - $z$  and  $y$ - $z$  planes looks like the quadrupole emission proportional to  $\sin^4 \theta$ , which is also the case in Stark and Piran. The total energy radiated at  $t = 30M_\odot$  observed at  $r = 20M_\odot$  are  $5.7 \times 10^{-7}M_\odot$ ,  $3.8 \times 10^{-6}M_\odot$ ,  $1.5 \times 10^{-5}M_\odot$  and  $3.6 \times 10^{-5}M_\odot$  for ROT1, ROT2, ROT3 and ROT4, respectively. Stark and Piran found that the total energy of gravitational waves is proportional to  $a^4$  for small  $a$  and it levels off at  $a \sim M_g$ . The same dependency reappears in our calculation; the total energy is expressed approximately

$$E_{GW} = 5 \times 10^{-5} \left( \frac{a}{M_g} \right)^4. \quad (85)$$

We have to remark that the value of the coefficient in Stark and Piran is about 20 times larger than ours. However, this is not disagreement, because Stark and Piran pursued their calculation up to  $t = 100M$  while we did only up to  $t = 30M$ . The energy we observed is thus just expected from the time dependence of the gravitational wave energy given by Stark and Piran [15].

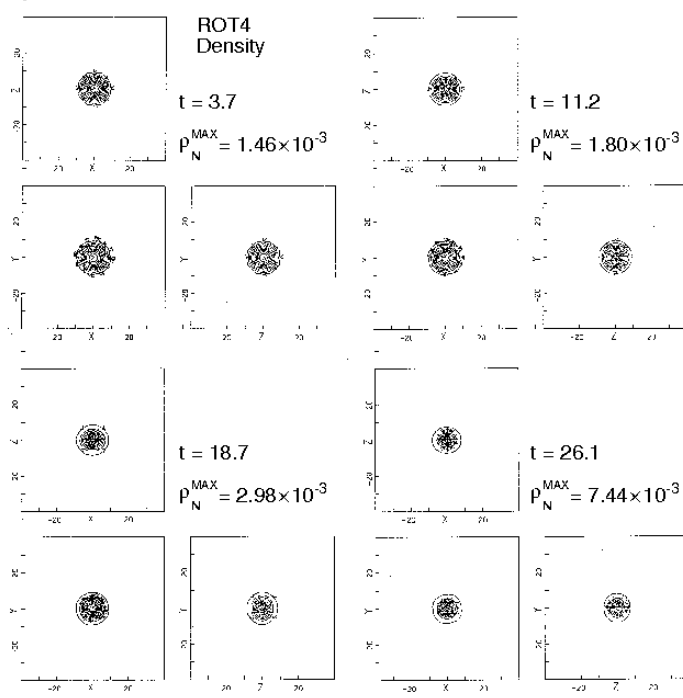


Fig. 12. — Mass density  $\rho_N$  on the  $x$ - $y$ ,  $y$ - $z$  and  $x$ - $z$  planes for a spherically symmetric collapse of a rotating star ROT4. Arrows indicate the velocity vector  $V^i$ .

### 3.3.3. Coalescing Binary Neutron Stars

Now we begin to attack the problem of coalescing binary neutron stars. We place as initial data two spherical neutron stars of mass  $M = 1.0M_\odot$  and radius  $r_0 = 6M$  with density distribution ( $\rho_N$ ) of  $\gamma = 2$  polytrope at  $x = r_0$  and  $x = -r_0$ ; two stars just touch each other. We add a rigid rotation with angular velocity  $\Omega$  as well as an approaching velocity  $v_a$  to this system such that

$$v_x^N = \begin{cases} -\Omega y - v_a & \text{if } x > 0, \\ -\Omega y + v_a & \text{if } x < 0, \end{cases} \quad (86)$$

$$v_y^N = \Omega x, \quad (87)$$

setting  $v_a = \Omega r_0$ .

We performed three simulations, BI1, BI2 and BI3, with different values of  $\Omega$ . The total angular momentum divided by the square of the gravitational

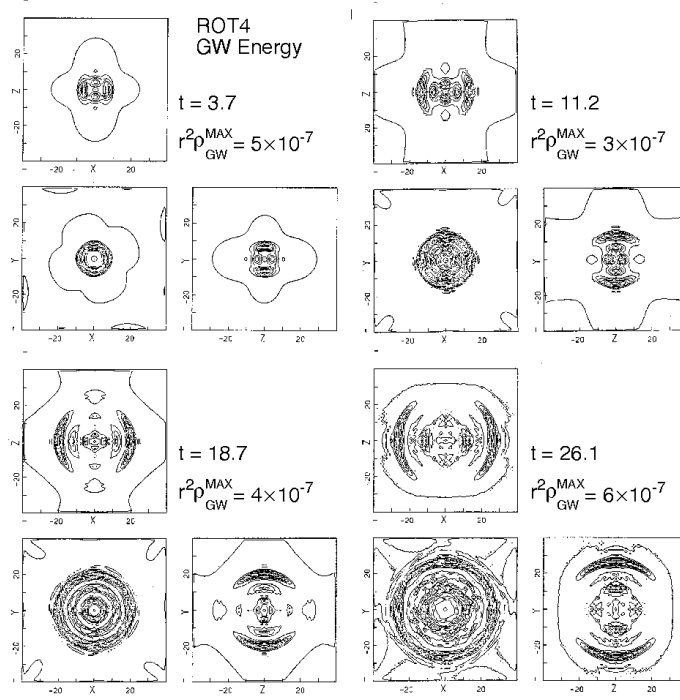


Fig. 13. — “Energy density of the gravitational waves”  $r^2 \rho_{GW}$  for ROT4.

mass are 0.71, 1.43 and 1.01 for BI1, BI2 and BI3, respectively.

Figure 14 shows the evolution of the density on the  $x$ - $y$ ,  $y$ - $z$  and  $x$ - $z$  planes of BI3. The final object will be a rotating black hole although we have not yet tried to determine the apparent horizon. The “gravitational wave energy”  $\rho_{GW}$  shows an interesting feature of generation and propagation of the waves. A spiral pattern appears on the  $x$ - $y$  plane while different patterns with peaks around  $z$ -axis appear on the  $x$ - $z$  and  $y$ - $z$  planes. This can be explained naively by the quadrupole wave pattern given by

$$r^2 \rho_{GW} = \frac{r^2}{32\pi} (A_{ij}^{TT})^2 \propto \cos^2 \theta + \sin^2 \theta \sin^2(2\Omega(t-r) - 2\varphi)/4. \quad (88)$$

On the  $x$ - $y$  plane, where  $\theta = \pi/2$ ,  $\rho_{GW}$  is constant along the spiral of  $r + \varphi/\Omega = \text{constant}$ , while near  $z$ -axis, where  $\theta \approx 0$ ,  $\rho_{GW} \propto \cos^2 \theta$ .

At the numerical boundary, we have to impose the outgoing wave condition to  $\tilde{\gamma}_{ij}$  and  $K_{ij}$ . In the present calculation, however,  $x_{\text{max}}$ ,  $y_{\text{max}}$  and  $z_{\text{max}}$  are comparable to the wave length of the expected gravitational waves,  $\sim 40M_{\odot}$ . We tried various boundary conditions, but none works well. We therefore adopt

a simple extrapolation at the numerical boundary and suspend calculations when the gravitational waves reach the numerical boundary. We hope that the problem will be overcome if the numerical boundary is located farther, where the outgoing wave condition becomes appropriate.

The total energy of the gravitational radiation amounts to  $3 \times 10^{-3} M_{\odot}$  at  $t = 35 M_{\odot}$  for BI3.

### Acknowledgments

This work is supported by the Grant-in-Aid for Scientific Research on Priority Area of Ministry Education (04234104).

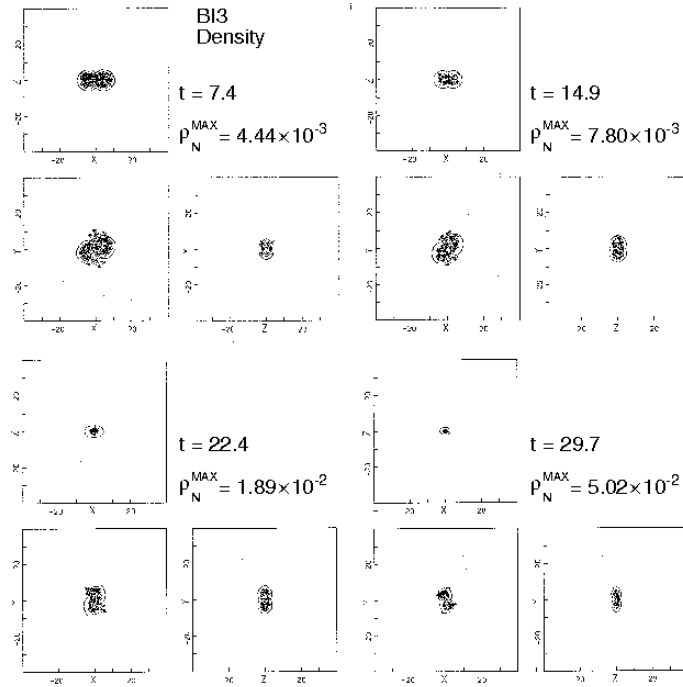


Fig. 14. — Density on the  $x$ - $y$ ,  $y$ - $z$  and  $x$ - $z$  planes for BI3. Arrows indicate the velocity vector  $V^i$ .

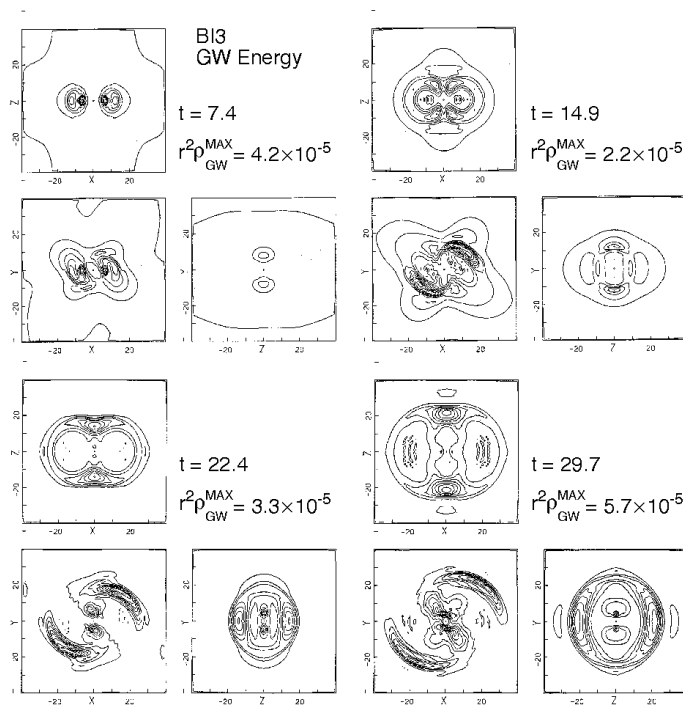


Fig. 15. — Energy density of the gravitational waves  $r^2 \rho_{\text{GW}}$  on the  $x$ - $y$ ,  $y$ - $z$  and  $x$ - $z$  planes for B13.

## References

- [1] Misner, C.W., Thorne, K.S., Wheeler, J.A., Gravitation (W.H. Freeman and Company, San Francisco, 1973) p. 993.
- [2] Blanchet, L., Damour, T. & Schäfer, G., *Mon. Not. R. Astron. Soc.* **241** (1990) 289.
- [3] Finn, L.S., *Frontiers of Numerical Relativity* (Cambridge University Press, Cambridge, 1989) p. 126.
- [4] van Leer, B., *J. Comput. Phys.* **23** (1977) 276.
- [5] Harten, A., *J. Comput. Phys.* **49** (1983) 357.
- [6] Oohara, K., Nakamura, T., *Approaches to Numerical Relativity* (Cambridge University Press, Cambridge, 1992) p. 182.
- [7] Meijerink, J.A., van der Vorst, H.A., *Math. Comp.* **31** (1977) 148.
- [8] Gustafsson, I., *BIT* **18** (1978) 142.
- [9] Ushiro, Y., *Kokyuroku of RIMS* **514** (1984) 110,(in Japanese).
- [10] van der Vorst, H.A., *Comput. Phys. Comm.* **53** (1989) 223.
- [11] Murata, K., Oguni, T., Karaki, Y., *Supercomputer* (Maruzen, Tokyo, 1985) p. 141,(in Japanese).
- [12] Oohara, K., Nakamura, T., *Prog. Theor. Phys.* **82** (1989) 535.
- [13] Nakamura, T., Oohara, K., *Frontiers of Numerical Relativity* (Cambridge University Press, Cambridge, 1989) p. 254.
- [14] Smarr, L., *Source of Gravitational Waves* (Cambridge University Press, Cambridge, 1979) p. 245.
- [15] Stark, R., Piran, T., *Phys. Rev. Lett.* **55** (1985) 891.  
Dynamical Spacetimes and Numerical Relativity (Cambridge University Press, Cambridge, 1985) p. 40.
- [16] Shibata, M., Nakamura, T., Oohara, K., *Prog. Theor. Phys.* **88** (1992) 1079.
- [17] Ipser, J., Managan, R., *Astrophys. J.* **250** (1981) 362.
- [18] Nakamura, T., Oohara, K., Kojima, Y., *Prog. Theor. Phys. Suppl.* **90** (1987) .
- [19] York Jr., J.W., *Source of Gravitational Radiation* (Cambridge University Press, Cambridge, 1979) p. 83.
- [20] York Jr., J.W., *J. Math. Phys.* **14** (1973) 456.
- [21] Shibata, M., Nakamura, T., *Prog. Theor. Phys.* **88** (1992) 317.
- [22] York Jr., J.W., Smarr, L., *Phys. Rev.* **D17** (1978) 1945.